the wiggler in which the interaction between laser and electron occurs. For a bend magnet located immediately following the wiggler (as shown in Fig. 1), the stretching of the electron distribution due to time-of-flight effects will be reduced by a factor of 3, resulting in an x-ray pulse duration of ~100 fs. In addition, the temporal structure of the electron distribution will give rise to the emission of a single-cycle infrared pulse ($\lambda_o \sim 120$ μm) that is spatially and temporally coherent (*12, 19*).

The average flux and brightness of the femtosecond x-rays can be determined from the full beamline flux and brightness scaled by three factors: $\eta_1 = \tau_L/\tau_e$, $\eta_2 = f_L/f_B$, and $\eta_3 \approx 0.2$, where τ_L and τ_e are the laser pulse and electron bunch durations, respectively; f_L and f_B are the laser and electron bunch repetition rates, respectively; and η_3 accounts for the fraction of electrons that are in the proper phase of the laser pulse to get the maximum energy exchange suitable for creating the large transverse separation. Synchrotron radiation damping provides for recovery of the electron beam between interactions. As the laser interacts sequentially with each bunch, the time interval between interactions is given by N_B/f_L, where N_B is the number of bunches in the storage ring. Furthermore, because the bunch slice is only a small fraction of the total bunch, an interaction interval of ~3 ms [30% of the storage ring damping time (*13*)] is sufficient to allow recovery of the electron beam between laser interactions (*9*). Thus, with 300 bunches in the storage ring, femtosecond x-rays can be generated at repetition rates as high as 100 kHz without adversely affecting the other beamlines at the ALS. On the basis of the known parameters of an ALS bend magnet and undulator at a beam energy of 1.9 GeV (*13, 20*), with $\eta_1\eta_2\eta_3 \approx 10^{-8}$ (for example, laser pulses of 25 fs, 100 μJ at 20 kHz), we expect an average femtosecond flux from a bend magnet of $\sim 10^5$ photons s^{-1} per 0.1% bandwidth (BW) (for a collection angle of 1 mrad) and an average brightness of $\sim 4 \times 10^7$ photons s^{-1} $mrad^{-2}$ mm^{-2} per 0.1% BW at a photon energy of 2 keV. For an ALS small-gap undulator, the average femtosecond flux is $\sim 10^7$ photons s^{-1} per 0.1% BW, and the average brightness is $\sim 10^{11}$ photons s^{-1} $mrad^{-2}$ mm^{-2} per 0.1% BW at a photon energy of 2 keV.

The generation of femtosecond x-rays is an important capability for third-generation synchrotron sources and promises to be a powerful tool for investigating ultrafast structural dynamics in materials. As this approach creates femtosecond time structure on the electron beam, standard radiating devices (bend magnet, wiggler, or undulator) can be designed to emit femtosecond x-ray pulses with the desired properties (bandwidth, tunability, brightness, and so forth). The x-ray flux and brightness levels available from such a femtosecond synchrotron source will enable a wide range of x-ray techniques, including diffraction and EXAFS, to be applied on a 100-fs time scale to investigate atomic motion associated with phase transitions in solids, making and breaking of bonds during chemical reactions, and possibly ultrafast biological processes.

References and Notes

1. T. Elsaesser, J. G. Fujimoto, D. A. Wiersma, W. Zinth, Eds., *Ultrafast Phenomena XI*, vol. 63 of *Springer Series in Chemical Physics* (Springer-Verlag, Berlin, 1998).
2. S. M. Mini, Ed., *Applications of Synchrotron Radiation Techniques to Materials Science IV*, vol. 524 of *Materials Research Society Symposia Proceedings* (Materials Research Society, Warrendale, PA, 1998).
3. A. M. Lindenberg *et al.*, *Phys. Rev. Lett.* **84**, 111 (2000).
4. C. Rischel *et al.*, *Nature* **390**, 490 (1997).
5. C. W. Siders *et al.*, *Science* **286**, 1340 (1999).
6. I. V. Tomov, D. A. Oulianov, P. Chen, P. M. Rentzepis, *J. Phys. Chem. B* **103**, 7081 (1999).
7. R. W. Schoenlein *et al.*, *Science* **274**, 236 (1996).
8. A. H. Chin *et al.*, *Phys. Rev. Lett.* **83**, 336 (1999).
9. A. A. Zholents and M. S. Zolotorev, *Phys. Rev. Lett.* **76**, 912 (1996).
10. C. Limborg, in *Time Structure of X-ray Sources and Its Applications*, A. K. Freund, H. P. Freund, M. R. Howells, Eds., vol. 3451 of *Proceedings of SPIE* (SPIE Press, Bellingham, WA, 1998).
11. D. E. Alferov, Y. A. Bushmakov, K. A. Belovintsev, E. G. Bessonov, P. A. Cherenkov, *Particle Accel.* **9**, 223 (1979).
12. R. W. Schoenlein *et al.*, *Appl. Phys. B*, in press.
13. "1–2 GeV Synchrotron Radiation Source—Conceptual Design Report," *LBL PUB-5172 Rev.* (Lawrence Berkeley Laboratory, Berkeley, CA, 1986).
14. The laser system consists of a Kerr lens mode-locked oscillator, pulse stretcher, multipass amplifier, and pulse compressor. For a review of similar laser systems, see S. Backus, C. G. Durfee, M. M. Murnane, H. C. Kapteyn, *Rev. Sci. Instrum.* **69**, 1207 (1998).
15. M. J. W. Rodwell, D. M. Bloom, K. J. Weingarten, *IEEE J. Quantum Electron.* **25**, 817 (1989).
16. A. Amir and Y. Greenzweig, *Nucl. Instrum. Methods Phys. Res. A* **250**, 404 (1986).
17. For x-rays, the relatively small collection angle of the beamline is more than sufficient to accurately image the source (electron beam) without being limited by diffraction.
18. Measurements of the electron beam profile at the ALS verify that it follows a Gaussian distribution out to $5\sigma_x$, corresponding to a background level of $\sim 10^{-6}$. Measurements of the x-ray beam profile at the image plane of a toroidal imaging mirror demonstrate that the nonspecular scattering in the horizontal plane can be suppressed to $\sim 10^{-4}$ of the peak specular intensity.
19. The field of the coherent single-cycle infrared pulse will correspond exactly to the solid line in Fig. 4A (minus the constant offset), and the flux will scale as the square of the number of absent electrons in the hole or dark pulse.
20. At 1.9 GeV, the average flux from an ALS bend magnet is $\sim 2 \times 10^{13}$ photons s^{-1} per 0.1% BW (for a collection angle of 1 mrad), and the average brightness is $\sim 5 \times 10^{15}$ photons s^{-1} $mrad^{-2}$ mm^{-2} per 0.1% BW at a photon energy of 2 keV. For an ALS small-gap undulator, the average flux is $\sim 10^{15}$ photons s^{-1} per 0.1% BW, and the average brightness is $\sim 10^{19}$ photons s^{-1} $mrad^{-2}$ mm^{-2} per 0.1% BW at a photon energy of 2 keV.

21. This work was supported by the U.S. Department of Energy under contract DE-AC03-76SF00098. The ALS is supported by the Director, Office of Science, Office of Basic Energy Sciences, and Materials Sciences Division of the U.S. Department of Energy under contract DE-AC03-76SF00098 at Lawrence Berkeley National Laboratory. We gratefully acknowledge the use of beamline 6.3.2 and the protein crystallography wiggler (W16) at the ALS and the technical assistance from the ALS Accelerator Physics Group, the ALS Engineering Group, and the ALS operations staff.

17 September 1999; accepted 8 February 2000

A Class of Microstructured Particles Through Colloidal Crystallization

Orlin D. Velev,* Abraham M. Lenhoff, Eric W. Kaler

Microstructured particles were synthesized by growing colloidal crystals in aqueous droplets suspended on fluorinated oil. The droplets template highly ordered and smooth particle assemblies, which diffract light and have remarkable structural stability. The method allows control of particle size and shape from spheres through ellipsoids to toroids by varying the droplet composition. Cocrystallization in colloidal mixtures yields anisotropic particles of organic and inorganic materials that can, for example, be oriented and turned over by magnetic fields. The results open the way to controllable formation of a wide variety of microstructures.

The study of colloidal crystals has provided important fundamental insights into colloidal forces and self-organization (*1*, *2*), and the crystals have promise as precursors for advanced materials. Closely packed crystals display a number of potentially usable characteristics such as light diffraction and photonic band gaps (*2–4*), high packing density and surface-to-volume ratio, maximal structural stability, and high catalytic/reactivity throughput. A major barrier to technological application of these structures is the lack of simple, easily controlled methods for mounting or shaping the crystals into usable solid objects.

Here we describe a method to template closely packed colloidal crystals into porous

Center for Molecular and Engineering Thermodynamics, Department of Chemical Engineering, University of Delaware, Newark, DE 19716, USA.

*To whom correspondence should be addressed. E-mail: velev@che.udel.edu

particles. Conventional methods for forming porous particles include stage-templated suspension polymerization (*5*), spray drying or drying in oil (*6*), sintering or dry impact blending (*7*), or aggregation in solution (*8*). Particles made by these methods are generally polydisperse or irregular, lack long-range ordering of the pores, and display a wide pore-size distribution that is not desirable for applications such as size-exclusion chromatography (*5*) and that decreases the mechanical stability of the particles. Nanoporous particles of narrow pore-size distribution have been synthesized by templating with self-assembled surfactant phases (*9*, *10*), but this method has yet to be extended to larger pore sizes.

Few methods for forming structured particles by assembly of smaller particles produce aggregates with long-range order. Ordered shells have been assembled from monodisperse micrometer-sized latex particles by the use of emulsion droplets as templates (*11*), but only two-dimensional (2D) polydisperse assemblies form, and the scheme for their production is relatively complex. An alternative approach has been to use droplets for the assembly of larger objects by the use of capillary forces (*12*). This method, however, requires large, specially prefabricated objects, and the assemblies are not structured or porous on a submicrometer level.

In the method outlined here, suspended droplets were used as templates within which the colloidal particles were gradually concentrated by drying to form 3D crystals, yielding a variety of microstructured symmetric supraparticles. Aqueous droplets of colloidal suspension were placed on the surface of perfluoromethyldecalin, an inert, dense (1.95 g/cm^3) liquid immiscible with water (Fig. 1). The droplets, of initial volume of a few microliters, contained 5 to 30 volume % (vol %) suspensions of negatively charged polystyrene latex microspheres 270 to 630 nm in diameter (*13*). To ensure the absence of strongly curved oil menisci at the walls of the container, which could attract and deform the droplets through capillary forces (*14*), we lined the inside of the Petri dish holding the oil with thin Teflon tape. The menisci formed in this way tended to attract the floating droplets gently to the walls, where they remained in contact with the surrounding Teflon tape but without noticeable deformation. The dish with the fluorinated oil was kept in a sealed chamber that contained a desiccating agent to drive removal of the water from the suspended droplets. The droplets shrank and ordered structures formed inside them within the first 2 to 4 hours of the incubation. After 12 hours, the crystalline porous particles were extracted and dried of oil.

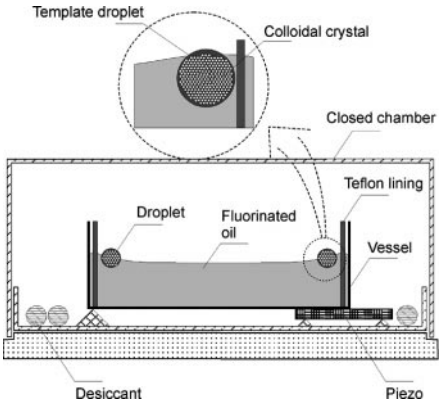

Fig. 1. Schematic of the assembly method. The template aqueous droplets are suspended on the surface of fluorinated oil and colloid crystals form during the drying process, as described in the text.

The initial experiments were carried out with 1- to 2-μl droplets of relatively high latex content (20 to 30 vol %). The assembly process yielded smooth spherical assemblies 100 to 500 μm in diameter and of very low density. Low-magnification optical microscopy shows brightly colored reflecting patches on the surface of these balls (Fig. 2). The colors depend on the size of the latex particles used: green and red for assemblies made of 270-nm microspheres, blue for 320-nm microspheres, and yellow-green for 630-nm microspheres. All porous supraparticles within a given batch displayed excellent homogeneity in size and appearance. The colors arise from light diffraction (opalescence) from the colloidal arrays, indicating long-range ordering of the latex particles, which can be visualized directly by scanning electron microscopy (SEM) (Fig. 3). Large domains of hexagonally packed particles are seen on the surface; each domain incorporates hundreds to thousands of microspheres in the first visible layer (Fig. 3A). The overall curvature of the porous balls is expressed in the dislocations between the different domains, but because of the large difference between the ball curvature and the latex diameter, the surface appears perfectly smooth on length scales comparable to the ball size. The size of the monocrystalline domains is comparable to those in the closely packed crystalline arrays obtained by slow evaporation or filtration of films from latex suspensions. However, the assemblies exhibit an almost complete absence of square arrays, which are commonly observed with planar crystals obtained by filtration or sedimentation [see, for example, (*2*, *15*)].

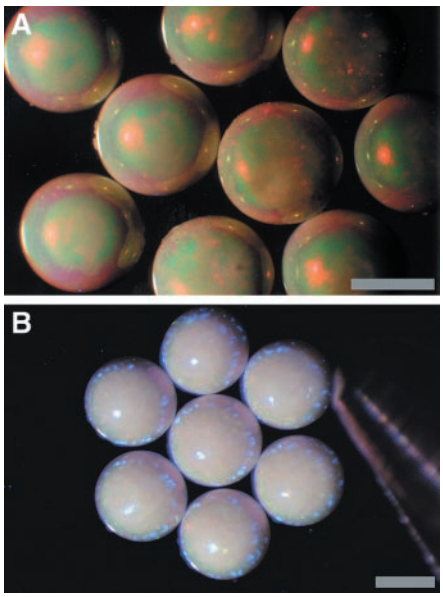

Fig. 2. Optical micrographs of structured spherical assemblies obtained from (**A**) 270-nm and (**B**) 320-nm latex particles. Scale bars, 500 μm.

The structure of the latex particles inside the porous balls can be observed along the edges of broken particles (Fig. 3B). The long-ranged ordered structure on the surface (top half) continues through the bulk of the ball and usually down to its center. The types of phases seen—coexisting randomly stacked hexagonal closely packed planes and face-centered cubic lattices—are similar to those reported earlier for bulk colloidal crystals (*1*, *2*, *15*). In contrast to crystals on solid surfaces, arrays of body-centered cubic packing are usually not observed. The absence of square arrays on the surface and in the bulk is probably due to the increased mobility of the particles adjacent to the nonsticky fluid drop surface, which allows better reorientation of the lattices during drying, and assembly into the more thermodynamically stable hexagonal phase. We showed that free rearrangement is a major factor favoring the for-

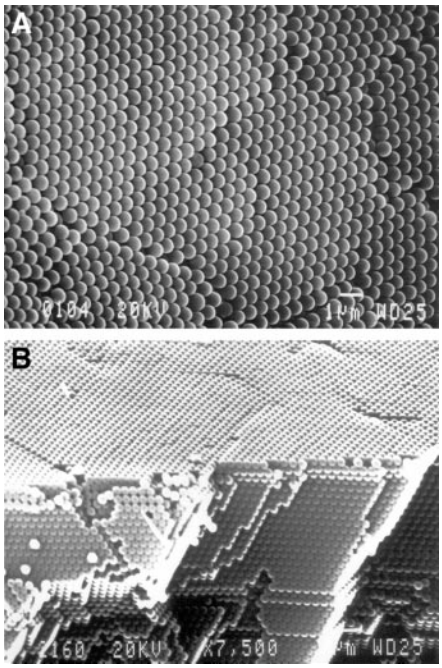

Fig. 3. (**A**) A scanning electron micrograph of a typical area on the surface of the assemblies. (**B**) A scanning electron micrograph along the edge of a broken particle. The surface is seen at the top and the cut through the bulk is toward the bottom of the micrograph. Scale bars, 1 μm.

mation of well-ordered crystals, both by addition of electrolyte, which decreases the quality of the arrays by decreasing the particle repulsion, and by gentle ultrasound treatment, which improves the structure by enhancing the rearrangement (*16*). The high packing density and order possibly contribute to the structural stability of the assemblies, which remain intact after mild to moderate mechanical manipulation and compression in both air and water. In contrast, the typical disordered latex aggregates obtained from suspension coagulation easily break into powder in air and spontaneously disassemble under water.

Our method allows control of the shape of the suspended template droplets by the interplay of droplet size, gravitational force, and interfacial tensions. The shape of a floating droplet (or lens) in general is given by the solution of the Laplace differential equation (*17*). The parameter that characterizes droplet deformation is the Bond number $\beta = (\Delta\rho g b^2)/\gamma$, where $\Delta\rho$ is the difference in the densities of the droplet and the surrounding fluid, g is the gravitational acceleration, b is the characteristic size of the droplet, and γ is the interfacial tension (*17*). The droplet is nearly spherical at values of $\beta \rightarrow 0$ and flattens as the value of β increases. Different values of β at the lower and upper droplet interfaces can be set experimentally by varying the relative densities of the fluids or by adding appropriate surfactants. The interfacial tensions in our system in the absence of surfactant are $\gamma_{water\text{-}air} = 72$ mN/m, $\gamma_{water\text{-}oil} = 53$ mN/m, and $\gamma_{oil\text{-}air} = 19$ mN/m (*18*). As the tension at the water-air boundary is about equal to the sum of the tensions at the other two interfaces, the droplet will have a smooth boundary at the three-phase contact line rather than a sharp contact edge (*17*). For 1-μl template droplets of pure liquids in our system, $\beta < 0.05$, and thus the droplet shape will be essentially spherical. The water-fluorocarbon-air system provides a great degree of flexibility in independently controlling the interfacial tensions by the use of surfactants that adsorb exclusively on the different interfaces (*19*). For larger droplets in the presence of surfactants, values of $\beta > 1$ are accessible, and lenslike, discoidal, and ellipsoidal templates with various three-phase contact angles can be obtained. Detailed formulas for calculation of the shapes in all cases are available (*17*, *20*).

Major modifications of the particle shape also result from the coupling of hydrodynamics and particle accumulation during the drying/crystallization process. If the initial volume fraction of the microspheres in the droplets is close to the crystallization threshold of about 50 to 60 vol %, the assemblies obtained are close in size and shape to those of the original droplets. However, if the latex concentration is below about 20%, the particles accumulate at the droplet periphery during water evaporation, which leads to subsequent deviations from a spherical shape. The shape of the assemblies then evolves from spherical (for small droplets) to flattened disks or ellipsoids for larger (>3 μl) droplets. An example of how the aspect ratio of such assemblies can be varied by altering the latex volume fraction is shown in Fig. 4A.

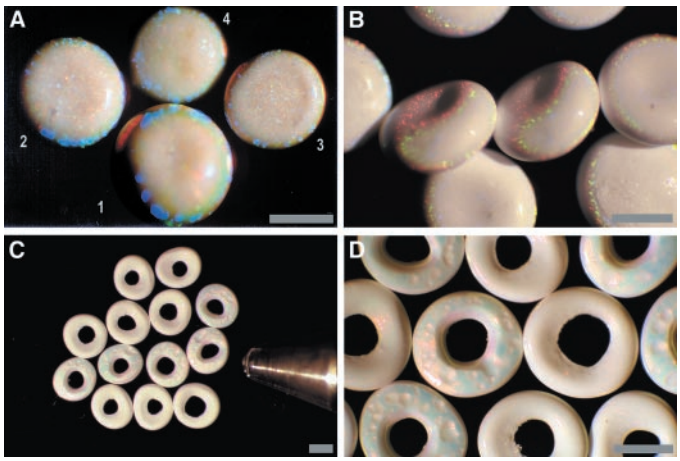

Fig. 4. Examples of shape control during assembly. (**A**) Assemblies from suspensions with latex concentrations of (1) 10%, (2) 6.7%, (3) 4%, and (4) 2.4%. Particle 1 is a sphere with flattened top and bottom, whereas all of the others are discs with different thicknesses. The focal plane is adjusted below the top of particle 1 and above the top of particle 4, showing the variation in the thickness. (**B**) Dimpled particles in the presence of fluorinated surfactant. (**C** and **D**) Toroidal, doughnutlike assemblies formed at higher surfactant concentration. Scale bars, 500 μm. Supplementary material with additional examples of variation of the shape and appearance of the particles is available at *Science* Online (*25*).

Further control of the shape can be achieved by adding surfactants to vary the interfacial tensions. Addition of a fluorinated surfactant, sodium perfluorooctanoate, led to formation of unexpectedly complex particles. Droplets containing 0.006 mM surfactant first flatten and then develop a dimple in the middle as they dry, ultimately yielding concave particles shaped like red blood cells (Fig. 4B). At higher surfactant concentrations (0.05 mM), the dimples between the two opposing surfaces bridge to form a hole. These dried assemblies are submillimeter toroids, or crystalline "doughnuts" (Fig. 4, C and D). The latex microspheres in the doughnuts are as well ordered as those in the spherical or the discoidal supraparticles, and the doughnuts also demonstrate the usual brightly colored diffraction patches on the surface (Fig. 4D). However, the lower interfacial tension caused by the surfactant allows some formation of steps between the bordering domains on the surface. The formation and the shape of the toroids are readily controllable; the outer diameter depends on the initial droplet size and particle concentration, whereas the size of the inner hole depends on the surfactant concentration.

Another important practical feature of the method is that complex composite assemblies can be fabricated when the original drop contains a mixture of two or more different types of particles. For example, the segregation of two types of colloids during assembly yields complex anisotropic particles. Such particles were formed from mixtures of 420-nm regular polystyrene beads (white in color) and 670-nm paramagnetic latex microspheres [encapsulating 20 weight % (wt %) magnetite, which are brown]. The heavier magnetic particles could be separated by gravity alone, so anisotropic particles can be produced merely by gravitational separation of the components in the droplets. However, a much quicker and cleaner separation results from application of a constant magnetic field during the drying/crystallization process (*21*). Complete separation of the microparticles into the two hemispheres of the dried assembly is seen in Fig. 5A. A valuable property of such anisotropic particles is that they can be manipulated by electric or magnetic fields. For example, a magnetic field immediately orders and orients the bicolored magnetic balls (Fig. 5B). The arrays then flip and change the displayed face from white to brown and back as the gradient of the field is reversed.

Finally, mixtures of two particles of substantially different sizes can be used both to create interesting anisotropic assemblies and to study the dynamics of the process. We studied suspensions containing 8% of 270-nm latex microspheres and 0.005 wt % of 40-nm colloidal gold particles. The much smaller gold particles are carried through the interstices of the latex by the retreating water during the drying process. These particles are ultimately deposited, and aggregated, at the surface from which the last traces of water evaporate. The dried gold colloids form blackish metallic rings only on the side of the assemblies in contact with air. The result is an unconventional "glazed doughnut" structure (Fig. 5, C and D). As the formation of such assemblies is also guided by the wetting of the particles, our method can be modified to make particles of anisotropic wettability,

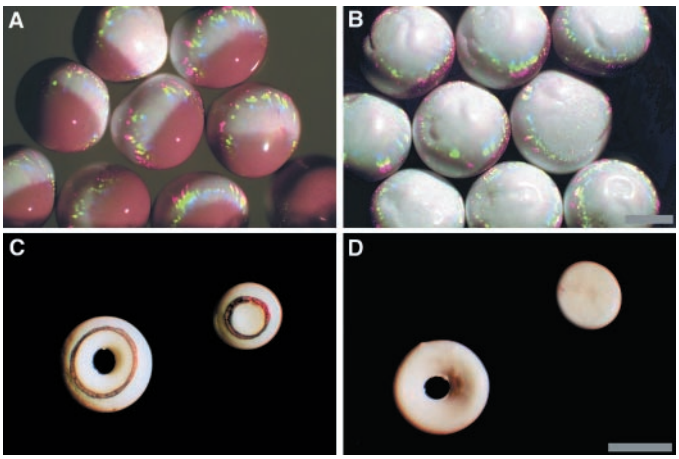

Fig. 5. Examples of anisotropic particles. (**A**) Unoriented spherical assemblies incorporating regular (white) and magnetic (brown) latexes. (**B**) In the presence of a magnetic field originating from below, these particles immediately form an array with the white halves oriented up. If the magnetic field gradient is reversed, the particles flip to form an array with the brown side up. (**C** and **D**) Two assemblies of complex shape obtained in the presence of small gold particles, as viewed from opposite faces. A metallic ring is deposited only on the side of the particle that was originally exposed to air. Scale bars, 500 μm.

broadly similar to the "Janus" beads demonstrated earlier (*22*).

Crystalline assemblies such as those reported here display long-ranged ordering of the constituting small particles that ensures uniform porosity and maximum mechanical stability and allows distinctive optical properties. The most unconventional feature of our method is the control of particle shapes and compositions. For example, the doughnuts may offer advantages in chromatography over the usual spherical particles by virtue of their combination of reduced mass transfer length scale, reduced pressure drop, and uniform porosity. Particles with magnetic and color anisotropy such as those shown in Fig. 5 can find application in switchable coatings, electronic paper (*23*), magnetooptical devices, or electrorheological or magnetorheological fluids. In addition to being anisotropic and magnetic, these particles are also of uniform porosity, monodisperse in size, and highly structured and can be produced in different shapes. All of these properties suggest areas for potential applications.

The variety of samples obtained warrants extension of the method to the formation of a wide range of particulate materials. Ideally, spherical particles can be assembled in droplets suspended in density-matched liquids (simulated microgravity conditions). The method can be modified for the assembly of inorganic particles from silica, TiO_2, ZrO_2, metals, or semiconductors. A wide variety of composites from organic, inorganic, and metallic particles are also possible. Anisotropic particles, responsive not only to magnetic but also to electric fields or light, can be created by such combinations. Another system of practical interest may be the combination of the droplet shape templating with colloidal crystal templating of structured lattices of pores (*24*). Thus, the structures reported here may be a prelude to a previously unidentified class of advanced particulate materials.

References and Notes

1. P. Pusey and W. van Megen, *Nature* **320**, 340 (1986); K. E. Davis, W. B. Russel, W. J. Glantschnig, *Science* **245**, 507 (1989); J. X. Zhu *et al.*, *Nature* **387**, 883 (1997); A. K. Arora and B. V. R. Tata, *Adv. Colloid Interface Sci.* **78**, 49 (1998).
2. N. A. Clark, A. J. Hurd, B. J. Ackerson, *Nature* **281**, 57 (1979); P. Pieranski, *Contemp. Phys.* **24**, 25 (1983).
3. I. I. Tahran and G. W. Watson, *Phys. Rev. Lett.* **76**, 315 (1996); W. L. Vos, M. Megens, C. M. van Kats, P. Boesecke, *J. Phys. Condens. Matter* **8**, 9503 (1996); A. van Blaaderen, *MRS Bull.* **39**, 39 (1998).
4. J. D. Joannopoulos, R. D. Meade, J. N. Winn, *Photonic Crystals: Molding the Flow of Light* (Princeton Univ. Press, Princeton, NJ, 1995).
5. F. Svec and J. M. J. Fréchet, *Science* **273**, 205 (1996).
6. C. Roth and R. Kobrich, *J. Aerosol Sci.* **19**, 939 (1988); K. Masters, *Spray Drying Handbook* (Longman, London, 1991); R. K. Iler and H. J. McQueston, U.S. Patent 3855172 (1972).
7. H. Egermann, *Powder Technol.* **27**, 203 (1980); H. Honda, M. Kimura, F. Honda, T. Matsuno, M. Koishi, *Colloids Surf. A* **82**, 117 (1994).
8. T. Sugimoto, *Adv. Colloid Interface Sci.* **28**, 65 (1987); L. F. Sun, M. J. Annen, F. Lorenzanoporras, P. W. Carr, A. V. McCormick, *J. Colloid Interface Sci.* **163**, 464 (1994).
9. S. Schacht, Q. Huo, I. G. Voigt-Martin, G. D. Stucky, F. Schüth, *Science* **273**, 768 (1996); P. T. Tanev and T. J. Pinnavaia, *Science* **271**, 1267 (1996); S. Mann and G. A. Ozin, *Nature* **382**, 313 (1996); H. Yang, N. Coombs, G. Ozin, *Nature* **386**, 692 (1997); Q. S. Huo, J. L. Feng, F. Schüth, G. D. Stucky, *Chem. Mater.* **9**, 14 (1997); D. Y. Zhao, P. D. Yang, Q. S. Huo, B. F. Chmelka, G. D. Stucky, *Curr. Opin. Solid State Mater. Sci.* **3**, 111 (1998).
10. P. J. Bruinsma, A. Y. Kim, J. Liu, S. Baskaran, *Chem. Mater.* **9**, 2507 (1997); M. Grun, I. Lauer, K. K. Unger, *Adv. Mater.* **9**, 254 (1997); Y. Lu *et al.*, *Nature* **398**, 223 (1999); C. J. Brinker, Y. Lu, A. Sellinger, H. Fan, *Adv. Mater.* **11**, 579 (1999).
11. O. D. Velev, K. Furusawa, K. Nagayama, *Langmuir* **12**, 2374 (1996); *Langmuir* **12**, 2385 (1996); O. D. Velev and K. Nagayama, *Langmuir* **13**, 1856 (1997).
12. A. Terfort, N. Bowden, G. M. Whitesides, *Nature* **386**, 162 (1997); W. T. S. Huck, J. Tien, G. M. Whitesides, *J. Am. Chem. Soc.* **120**, 8267 (1998); J. Tien, T. L. Breen, G. M. Whitesides, *J. Am. Chem. Soc.* **120**, 12670 (1998); T. L. Breen, J. Tien, S. R. J. Oliver, T. Hadzic, G. M. Whitesides, *Science* **284**, 948 (1999).
13. About 15 ml of perfluoromethyldecalin was poured into the Petri dish with an inner diameter of 50 mm. The surface of the oil in the dish was routinely cleaned by sweeping it with a large water droplet attached to the end of a pipette. Ten to 15 droplets of latex suspension were then deposited on the surface from a 10-μl microsyringe. Sulfate-functionalized regular latexes were obtained from IDC (Portland, OR), and carboxylate magnetic microspheres were obtained from Bangs Laboratories (Fishers, IN). Before the chamber was sealed, 2.5 to 3.5 g of desiccating agent (Drierite) was distributed around the vessel containing the fluorinated oil. The assemblies formed, together with a minimal amount of oil, were removed from the oil surface with a plastic pipette with an opening of about 2 mm and air-dried. The particles were observed with an Olympus BH-2 optical microscope equipped with a long-focus 4× objective and both transmitted and side illuminators. Structural characterization was carried out on a JEOL JXA-840 scanning electron microscope. The particles were mounted on SEM stubs, covered with a sputtered gold layer, and observed at accelerating voltages of 5 to 25 kV.
14. P. A. Kralchevsky, V. N. Paunov, I. B. Ivanov, K. Nagayama, *J. Colloid Interface Sci.* **151**, 79 (1992); P. A. Kralchevsky, V. N. Paunov, N. D. Denkov, K. Nagayama, *J. Colloid Interface Sci.* **167**, 47 (1994); O. D. Velev, N. D. Denkov, V. N. Paunov, P. A. Kralchevsky, K. Nagayama, *J. Colloid Interface Sci.* **167**, 66 (1994).
15. S. Neser, C. Bechinger, P. Leiderer, T. Palberg, *Phys. Rev. Lett.* **79**, 2348 (1997); O. D. Velev, T. A. Jede, R. F. Lobo, A. M. Lenhoff, *Chem. Mater.* **10**, 3597 (1998).
16. The electrolyte suppresses the electrostatic repulsion between the particles and leads to coagulation. The adverse effect of electrolyte was shown by adding 0.05 M NaCl to the initial particle suspension, which disrupted the ordering and eventually led to breakdown of the assembled particles. Conversely, the quality of the ordered array improved if a sound/ultrasound treatment was applied during the assembly process through a piezoelectric transducer attached to the bottom of the Petri dish. The application of a square wave of 11-kHz frequency noticeably improved the ordering of the microspheres both throughout the particle bulk and on the surface. However, this was also accompanied by an overall shape deformation in the area of contact with the Teflon wall.
17. H. M. Princen, in *Surface and Colloid Science*, E. Matijevic, Ed. (Wiley, New York, 1969), vol. 2, pp. 1–84.
18. M. Morita *et al.*, *Colloids Surf.* **67**, 81 (1992).
19. Hydrophilic-hydrocarbon surfactants are active at the air-water interface, ones with hydrophilic-fluorocarbon chains are active at the water–fluorinated oil interface, and hydrocarbon-fluorocarbon ones are active exclusively at the air–fluorinated oil interface (*18*).
20. F. M. Orr, L. E. Scriven, A. P. Rivas, *J. Fluid. Mech.* **67**, 723 (1975); P. Concus and R. Finn, Eds., *Variational Methods for Free Surface Interfaces* (Springer-Verlag, New York, 1987); J. S. Rowlinson and B. Widom, *Molecular Theory of Capillarity* (Oxford Univ. Press, Oxford, UK, 1989); R. Aveyard, J. H. Clint, D. Nees, V. Paunov, *Colloids Surf. A* **146**, 95 (1999).
21. A ceramic pot magnet of 82-mm diameter was placed 15 mm below the surface of the oil in the chamber. The paramagnetic particles are separated to the bottom of the template droplets within a few seconds.
22. C. Casagrande and M. Veyssié, *C. R. Acad. Sci. Paris II* **306**, 1423 (1988); C. Casagrande, P. Fabre, E. Raphaël, M. Veyssié, *Europhys. Lett.* **9**, 251 (1989); P.-G. de Gennes, *Angew. Chem. Int. Ed. Engl.* **31**, 842 (1992).
23. B. Comiskey, J. D. Albert, H. Yoshizawa, J. Jacobson, *Nature* **394**, 253 (1998).
24. O. D. Velev, T. A. Jede, R. F. Lobo, A. M. Lenhoff, *Nature* **389**, 447 (1997); B. T. Holland, C. F. Blanford, A. Stein, *Science* **281**, 538 (1998); J. E. G. J. Wijnhoven and W. L. Vos, *Science* **281**, 802 (1998); S. H. Park, D. Qin, Y. Xia, *Adv. Mater.* **10**, 1028 (1998); A. A. Zakhidov *et al.*, *Science* **282**, 897 (1998); P. Yang *et al.*, *Science* **282**, 2244 (1998).
25. Supplementary material is available at www.sciencemag.org/feature/data/1047430.shl.

26. We are grateful to N. L. Abbott and R. F. Lobo for useful discussions.

29 November 1999; accepted 10 February 2000